Nocturnal thermal structure of the mesosphere and lower thermosphere region at Maui, Hawaii (20.7°N), and Starfire Optical Range, New Mexico (35°N)

Xinzhao Chu, Chester S. Gardner, and Steven J. Franke
Department of Electrical and Computer Engineering, University of Illinois at Urbana-Champaign, Urbana, Illinois, USA

Received 10 April 2004; revised 21 October 2004; accepted 12 November 2004; published 29 January 2005.

[1] The nighttime thermal structure of the mesosphere and lower thermosphere (MLT) region at the Starfire Optical Range (SOR), New Mexico (35.0°N, 106.5°W), and at Maui, Hawaii (20.7°N, 156.3°W), are characterized using Na lidar observations. Both locations exhibit mesospheric temperature inversion layers (MILs) between 85 and 100 km that are not predicted by the MSIS-00 model. The amplitudes of the Maui MILs (~5.8 K) are about half of those at SOR (~9.8 K), and the Maui MILs have a smaller width (~11.1 km) compared to the SOR MILs (~14.5 km). The Maui lidar temperatures are generally warmer than the MSIS-00 predictions, while the SOR lidar data are comparable to the MSIS-00, except in the MIL altitude range. Both SOR and Maui mesopause temperatures are coldest in midsummer and are warmest during the mesopause transition periods. However, the Maui mesopause is warmer than the SOR, and the amplitude of the mesopause temperature variations at Maui (~9 K) is much smaller than at SOR (~19 K). Two distinct levels of mesopause altitudes are clearly shown in the SOR seasonal data with a low altitude around 86.5 km in summer (May through August) and a high altitude around 101 km during the rest of the year. Abrupt transitions between the two stable levels occur in early May and early September. The lidar measurements indicate a low mesopause altitude near 87.5 km in July at Maui when averaging over a 10-hour period centered at local midnight.

Citation: Chu, X., C. S. Gardner, and S. J. Franke (2005), Nocturnal thermal structure of the mesosphere and lower thermosphere region at Maui, Hawaii (20.7°N), and Starfire Optical Range, New Mexico (35°N), *J. Geophys. Res.*, *110*, D09S03, doi:10.1029/2004JD004891.

1. Introduction

[2] Observations of the thermal structure of the mesosphere and lower thermosphere (MLT) region are important for understanding atmosphere energetics and for calibrating atmospheric models. Extensive lidar measurements have been made in the Arctic [*Lübken and von Zahn*, 1991] and Antarctica [*Pan and Gardner*, 2003; *Kawahara et al.*, 2004], where the mesopause temperatures were observed to be more than 60 K colder in summer than in winter. Numerous lidar measurements have also been conducted at midlatitude [e.g., *Leblanc et al.*, 1998; *States and Gardner*, 2000; *She et al.*, 2000; *Chen et al.*, 2000; *Fricke-Begemann et al.*, 2002], where similar cold summer and warm winter temperatures were observed but with much smaller amplitudes for the seasonal variations. This difference has been attributed to the different strengths of the vertical motions associated with the meridional circulation at different latitudes. The vertical motions are expected to be strongest over the pole, weaker in the midlatitudes, and virtually nonexistent in the tropics [*Andrews et al.*, 1987]. Meanwhile, atmospheric tides and waves influence the MLT thermal structure with different modes, amplitudes, and phases at different latitudes [*Forbes*, 1995]. Therefore the tropical and subtropical thermal structures are expected to be different from those at middle and high latitudes. However, measurements of the MLT temperature are still rare in the low-latitude region. Only five lidar studies have been reported for low latitudes [*Gardner et al.*, 1995; *von Zahn et al.*, 1996; *Leblanc et al.*, 1998; *Clemesha et al.*, 1999; *Friedman*, 2003]. An empirical atmosphere model (mass spectrometer incoherent scatter model) has been developed from the CIRA-86 through the MSIS-90 to the MSIS-00 [*Hedin*, 1991; *Picone et al.*, 2002]. Their predictions were recently compared with observational data at the South Pole [*Pan and Gardner*, 2003] and at midlatitude in the northern hemisphere [*States and Gardner*, 2000]. However, comparisons with low-latitude measurements are rare.

[3] The University of Illinois Na wind/temperature lidar was coupled to large astronomical telescopes at the Starfire Optical Range (SOR) in Albuquerque, New Mexico (35.0°N, 106.5°W), and at the Maui Space Surveillance Complex on the top of the Haleakala in Maui, Hawaii (20.7°N, 156.3°W). The lidar measured temperature, wind (both vertical and horizontal), and Na density in the mesopause region as well as momentum and heat fluxes, and atmospheric instabilities. Hundreds of hours of high quality data have been collected at these two locations. This

0148-0227/05/2004JD004891$09.00

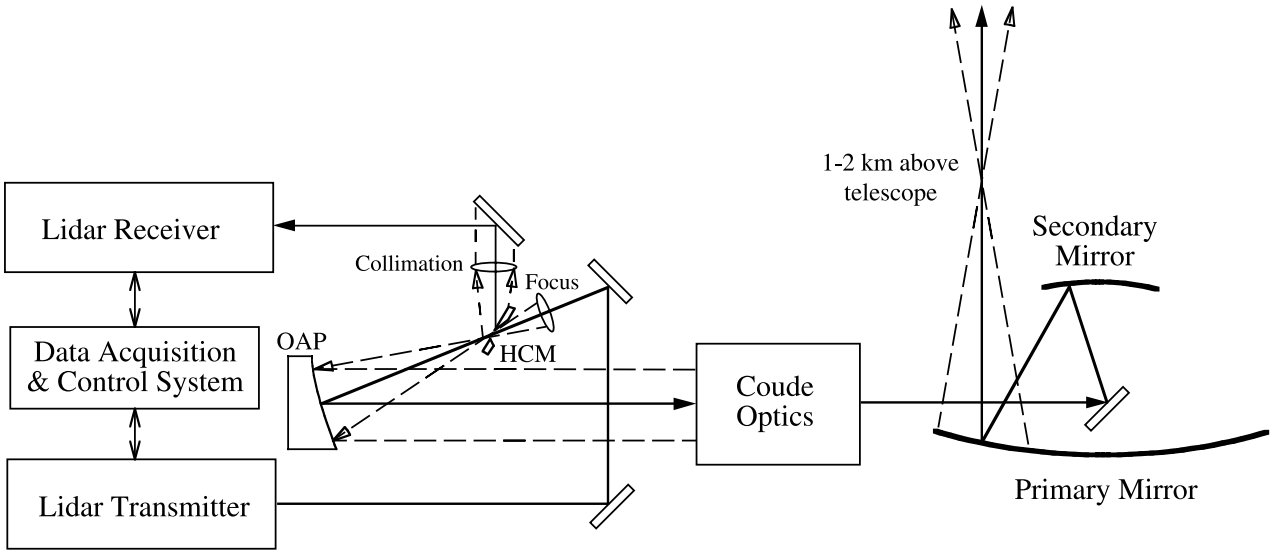

Figure 1. Schematic of the large-aperture steerable Na wind/temperature lidar system at SOR and Maui. OAP, off-axis-parabola; HCM, hole-coupling-mirror; Focus, focus/injection lenses; Collimation, collimating lenses. The diagram is not scaled.

provides a good opportunity to study the subtropical thermal structure of the MLT region and make comparisons with midlatitudes. In this paper we characterize the nocturnal mean background of the MLT thermal structure at Maui and SOR using the Na lidar data, and verify the differences and similarities between the low- and middle-latitude sites. We also compare the observations with the MSIS-00 model. The goal is to provide a better understanding of the energy budget of the MLT region.

2. Instrumentation

[4] The instrument employed at SOR and Maui is a large-aperture steerable Na wind/temperature lidar that can point precisely in any direction above 5° elevation. The steering ability is achieved by using the Coudé optics to project the lidar beam off a portion of the large primary mirror. A schematic of this steerable Na wind/temperature lidar is illustrated in Figure 1. The key optics are a hole coupling mirror (HCM), injection lens, and an off-axis parabolic mirror (OAP). As shown in Figure 1, the laser beam is focused and projected through the HCM to flood the OAP. The expanded laser beam is then directed by the OAP through the Coudé optics, tertiary and secondary mirrors, and then projected off-center onto the primary mirror of the telescope. Once the beam leaves the primary mirror, it is focused a few kilometers above the telescope, and then diverges to produce a large footprint at the Na layer altitude of 90 km. The backscattered photons are collected by the primary, and then directed through the same Coudé path to the OAP. The return beam has a different divergence than the outgoing beam and produces a spot much larger than the size of the hole at the HCM. The returned photons passing through the hole will be lost, but the rest of the signal is reflected by the HCM to the lidar receiver.

[5] The SOR telescope has a primary mirror of 3.5 m in diameter, a field-of-view (FOV) of 0.9 mrad full angle, and a short focal length of 315 m. The transmitted laser beam is reflected off a 1 m diameter spot on the SOR primary mirror, focused 1.1 km above the telescope, and produces a spot of 80 m in diameter (full width at e^{-2}) at 90 km. This gives an equivalent divergence of 0.9 mrad. The Maui AEOS telescope has a primary mirror of 3.67 m in diameter, a FOV of 0.44 mrad full angle, and a long focal length of 726 m. The transmitted laser beam is reflected off a 0.6 m diameter spot on the AEOS primary mirror, focused 2.2 km above the telescope, and produces a footprint of 40 m in diameter (full width at e^{-2}) at 100 km. The equivalent beam divergence is 0.4 mrad. The repetition rate of the Na lidar system was 30 Hz at SOR and 50 Hz at Maui. The lidar system parameters for the SOR and Maui installations are summarized in Table 1. Detailed descriptions of the Na lidar technique can be found in several papers [e.g., *Bills et al.*, 1991; *She et al.*, 1992; *Papen et al.*, 1995].

3. Observations

[6] The SOR observations were conducted in a monthly campaign mode. From June 1998 to November 2000, the Na lidar was operated at SOR for the week centered on new moon for every month. The goal was to collect approximately 40 hours of data per month in all 12 months.

Table 1. Comparison of SOR and Maui Na Wind/Temperature Lidar Parameters

Site	Primary Mirror Diameter, m	Telescope Focal Length, m	Field of View, mrad	Laser Spot on Primary, m	Focus Above Primary, km	Off Zenith Angle	Repetition Rate, Hz	Laser Pulse Energy, mJ	Integration Time, Number of Shots	Signal Level, Count per Shot
SOR	3.5	315	0.9	1	1.1	10°	30	40–50	900	1000–3000
Maui	3.67	726	0.44	0.6	2.2	30°	50	20–35	1500	250–1000

Table 2. Statistics of the Data Collection at SOR and Maui

	January	February	March	April	May	June	July	August	September	October	November	December	Total
							SOR						
Night	5	2	3	5	6	3	—	4	7	6	12	5	58
Hour	43.3	14.1	20.9	34.6	42.9	20.7	—	19.0	40.0	46.3	70.0	48.3	400.1
							Maui						
Night	6	—	—	5	—	—	7	—	—	7	—	—	25
Hour	31.5	—	—	37.4	—	—	44.1	—	—	51.8	—	—	164.8

Data were successfully collected during every month except July. Fifty-eight nights of data (about 400 hours) were obtained at SOR. The Maui observations were conducted in a seasonal campaign mode. The lidar was operated during two weeks around new moon in January, April, July, and October. From January 2002 to January 2004, six observational campaigns were conducted and total of 25 nights of data (about 165 hours) were obtained. Statistics of SOR and Maui data collection are summarized in Table 2. Plotted in Figure 2 are the histograms of day-of-the-year versus the observational hours per night (in local time) for SOR and Maui. During these campaigns, the lidar beam was pointed at zenith (Z) and off-zenith to the north (N), east (E), south (S), and west (W) in the sequence ZNEZSW. The off-zenith angle was 10° at SOR in order to measure both momentum flux and horizontal wind with reasonable accuracies, while a 30° off-zenith angle was used at Maui for better horizontal wind observations. Both zenith and off-zenith data are used in this study of the temperature profiles.

[7] A three-frequency technique was used to measure temperature and wind at both sites [*She and Yu*, 1994; *States and Gardner*, 2000]. The cw local-oscillator laser was locked to a Doppler-free hyperfine feature near the D_{2a} fluorescence line peak and an acousto-optic modulator was used to shift the laser frequency by ±630 MHz. In order to eliminate the effect of Na density fluctuations on the temperature and wind measurements, the lidar frequency was switched between these three frequencies every 50 laser pulses, i.e., the switching was done every 1.3 s at SOR (30 Hz repetition rate) and every 1 s at Maui (50 Hz repetition rate). At each frequency the signal was integrated for 900 laser pulses at SOR and 1500 laser pulses at Maui at a range resolution of 24 m. An integration time of 90 s is required for one complete profile containing observations at all three frequencies. It takes approximately 30 s to steer the telescope to the next position at both SOR and Maui. Thus to point the telescope and collect data takes about 2 min on average for each pointing direction. The pointing sequence ZNEZSW is completed every 12 min at both SOR and Maui. Owing to the large telescope apertures at both sites, the high photon signal levels result in a less than 1 K temperature error at the Na layer peak for 90-s integration and 480-m spatial resolution.

4. Monthly and Annual Mean Temperatures

[8] The lidar temperature data were averaged in local time for each month to derive the monthly mean background profiles. The temperature data of each individual night were first binned to fixed altitude and time with spatial and temporal resolutions of 500 m and 30 min, respectively. A composite night of data for each month was obtained by averaging the data in the same local time for different nights within each month. Then the composite night data were spatially and then temporally smoothed using Hamming windows with full widths of 2 km and 2 hours, respectively. The smoothing widths were chosen to remove most of the high frequency waves, while preserving the vertical and temporal structure of the MLT region for each month. The resulting monthly composite night usually covers most of the night from sunset to sunrise. Illustrated in Figure 3 are the January, April, July, and October composite nights obtained at Maui along with the corresponding data for SOR. Owing to the lack of July data at SOR, the June and August data were averaged in the same local time and then plotted against the Maui July data in Figure 3c. The time has been adjusted to the local solar time at each location. The universal time corresponding to the local midnight are 0706 and 1025 UT at SOR and Maui, respectively. For most months, observations cover the 10-hour period centered about local midnight. Monthly mean temperature profiles were then derived by averaging the monthly composite data

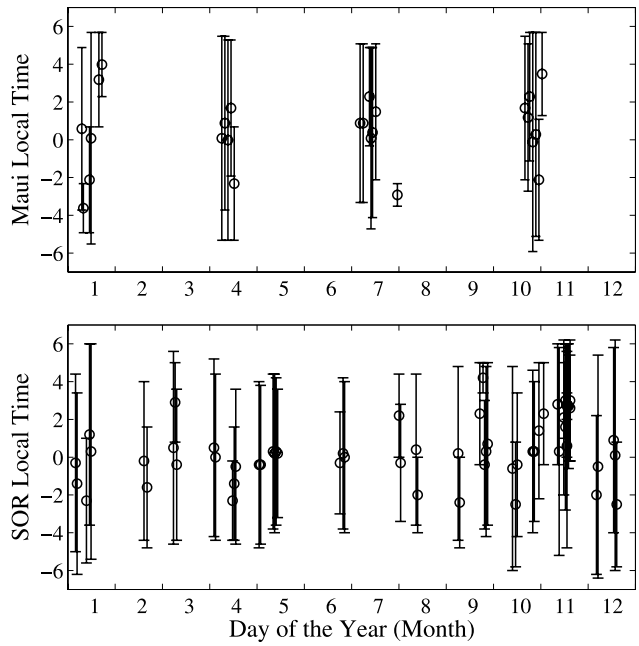

Figure 2. Histograms of the day-of-the-year versus the observational hours per night for (top) Maui and (bottom) SOR. The vertical lines indicate the start and stop time, while the circles indicate the center of the observation period.

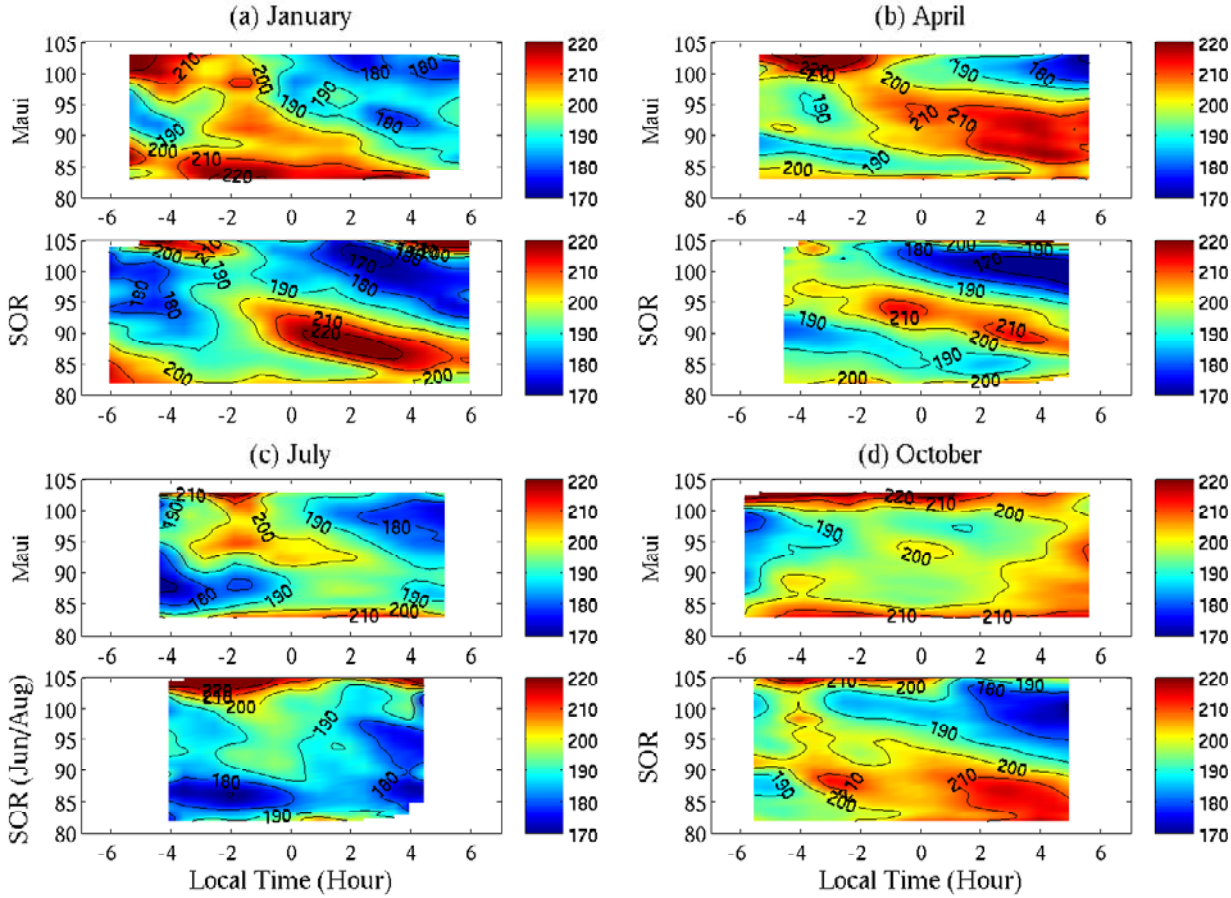

Figure 3. Comparisons of Maui and SOR monthly composite night temperatures in January, April, July, and October. The SOR July data were obtained by averaging the SOR June and August data.

within this 10-hour period. Plotted in Figures 4 and 5 are the monthly mean temperature profiles (black solid curves) for 11 months at SOR and 4 months at Maui, respectively. The corresponding numerical values of the monthly mean temperatures are listed in Tables 3 and 4.

[9] Plotted in Figure 6 are the annual composite nights obtained by averaging the monthly composite nights (shown in Figure 3) over 4 months at Maui and 11 months at SOR in the same local time. The annual mean temperatures were then derived by averaging the annual composite night over the 10-hour period centered about local midnight. The resulting Maui nocturnal annual mean is plotted as the solid curve in Figure 7. It is necessary to consider the effects of incomplete sampling on the annual means. There are only 4 months data at Maui and 11 months data at SOR. Using the MSIS-00 data to simulate the average at Maui, we found that the mean taken over the 4 months of January, April, July, and October is equal to the annual mean averaged over all 12 months. We also applied a harmonic fit containing an annual sinusoidal variation and a mean background to the 4 months of Maui lidar data. The fitted mean background is identical to the 4-month annual mean. Thus the annual mean obtained by lidar in the 4 months is likely to be close to the true annual mean over 12 months in the nighttime. However, the SOR data span 11 months. To derive a true annual mean for SOR, we applied a harmonic fit to the 11 monthly means of SOR temperatures. The fitting equation contains a mean background plus annual and semiannual sinusoidal variations. The harmonic fit was conducted at each altitude, and the resulting SOR mean background is plotted as the dashed curve in Figure 7. Compared with the mean of 11 months, the fitted mean background has a warmer mesopause around 100 km but a colder lower minimum around 85 km. This is expected as the coldest mesopause temperature (nighttime) occurs around 85 km in July while the temperature around 100 km in July is relatively warm, as observed in the midlatitudes [*States and Gardner*, 2000; *Chen et al.*, 2000]. The numerical values of the annual mean temperatures shown in Figure 7 are listed in Tables 3 and 4 for SOR and Maui, respectively.

[10] The geophysical variability of the monthly mean temperatures is indicated as the thin horizontal lines spanning the monthly mean temperature profiles in Figures 4 and 5, and the annual geophysical variability is indicated as the horizontal lines spanning the annual mean temperature profiles in Figure 7 where the red lines are for Maui and the blue for SOR. The monthly geophysical variability was obtained by computing the standard deviation of the monthly composite nights (shown in Figure 3) at each altitude, while the annual geophysical variability was obtained by computing the standard deviation of the annual composite night data (shown in Figure 6). Averaging in the same local time over different observational nights removes most of the noncoherent waves, such as gravity waves.

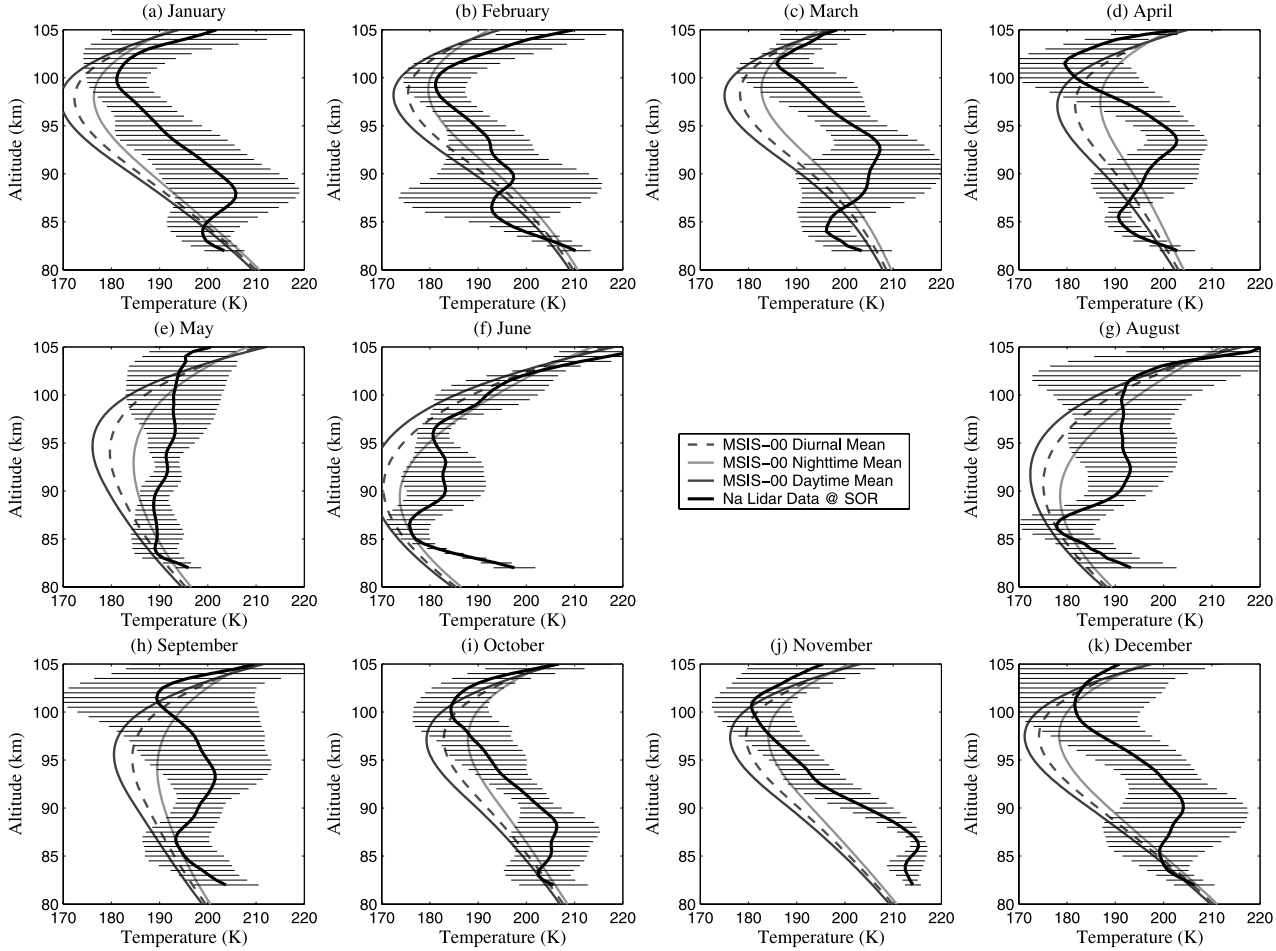

Figure 4. SOR nocturnal monthly mean background temperatures derived from monthly composite night data. Also plotted are the MSIS-00 diurnal, nighttime, and daytime mean in the same months at SOR for comparisons. The horizontal lines spanning the lidar monthly mean temperature profiles indicate the geophysical variability derived from the standard deviation of the monthly composite nights shown in Figure 3.

However, the coherent tides (e.g., the migrating tides with diurnal cycle and its harmonic) remain in the monthly and annual composite nights. Figures 3 and 6 clearly show the signatures of the diurnal and semidiurnal tides with downward phase propagation at SOR and Maui. The geophysical variances plotted in Figures 4, 5, and 7 mainly reflect the coherent tidal influences on the monthly and annual mean thermal structure. The typical standard deviation is about 5–10 K, with the maximum to 20 K and the minimum to a few K. Owing to the small number of samples, some long-period waves, such as planetary waves, may not be completely removed from the composite nights. Nevertheless, the main wave structures in the monthly and annual composite nights are from the coherent tides. These tides strongly influence the MLT thermal structure at SOR and Maui. To reveal the true mean background thermal structure, the tidal influences must be removed from the data. However, the limited 10-hour nighttime data do not allow us to precisely derive the tidal information, especially the 24-hour diurnal tides. Averaging over the 10-hour composite nighttime data removes most of the 12-hour tidal effects and other wave effects with periods less than 10 hours, but the approach is not sufficient to smooth out the 24-hour tidal influence. Therefore these monthly and annual mean temperatures shown in Figures 4, 5, and 7 should be regarded as the nocturnal thermal structures of the MLT region at Maui and SOR, which may differ from the true mean background of the MLT thermal structure. To completely remove the diurnal tides, observations covering the complete diurnal cycle are required.

4.1. Comparison With MSIS-00 Model

[11] Also plotted in Figures 4 and 5 are the monthly mean temperatures derived from the MSIS-00 model. Three means were computed from the MSIS model at each location: the 24-hour diurnal mean (red dashed curves), the nighttime mean corresponding to the same 10-hour period centered about local midnight as our lidar observational hours per night (green solid curves), and the daytime mean corresponding to the rest of the 14 hours centered about local noon (blue solid curves). Figures 4 and 5 indicate that the MSIS-00 model has included some tidal effects because the 10-hour nighttime mean is warmer than the 14-hour daytime mean by approximately 9 K at SOR and 12 K at Maui in the mesopause region. As expected, the MSIS-00 nighttime mean (green solid lines) is in better

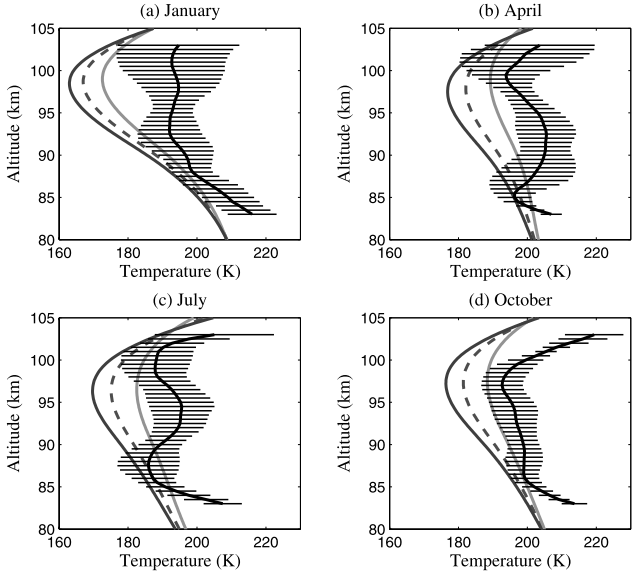

Figure 5. Maui nocturnal monthly mean background temperature derived from monthly composite night data. Also plotted are the MSIS-00 diurnal, nighttime, and daytime mean in the same months at Maui for comparison. The figure legends are the same as Figure 4.

agreement with the lidar observations than either the diurnal mean or the daytime mean.

[12] A striking feature in the monthly and annual means of the measured temperature profiles is the mesospheric temperature inversion layers (MIL) from 85 to 100 km. The MIL phenomenon was observed in all 11 months at SOR and 4 months at Maui. Therefore there are two temperature minima in the MLT region (80–105 km) for every month. These features are, however, not shown in any of MSIS-00 predictions. The MSIS-00 model predicts a single temperature minimum in the MLT region without any inversion layer regardless the time of day. Several lidar groups have reported the two temperature minima and inversion layers in the nighttime MLT region [e.g., *She et al.*, 1993; *States and Gardner*, 1998, 2000; *Meriwether et al.*, 1998]. However, when observations are averaged over the complete diurnal cycle, the inversion layers are nearly completely absent from the temperature profiles [*States and Gardner*, 2000]. It was suggested that this phenomenon is an artifact caused by incomplete sampling of the diurnal tide and nighttime chemical heating [*Mlynczak and Solomon*, 1993; *Meriwether et al.*, 1998; *States and Gardner*, 2000]. Therefore it is important to include the nighttime chemical heating effects in the future MSIS model to match these nighttime lidar observations.

[13] Outside the inversion layers, the SOR lidar temperatures are generally comparable to the MSIS-00 nighttime mean below 85 km with exceptions in June and November when the lidar temperatures are warmer than the MSIS-00. Above 100 km, the lidar temperatures are warmer than the

Table 4. Monthly and Annual Mean Temperature (K) at Maui

Altitude, km	January	April	July	October	Annual
103.0	194.7	203.6	205.0	219.4	205.9
102.0	193.1	199.5	192.8	212.1	199.7
101.0	192.7	197.3	188.8	205.4	196.3
100.0	193.3	194.5	188.2	199.5	194.1
99.0	194.2	194.0	187.9	195.4	193.0
98.0	194.7	195.7	188.6	193.3	193.1
97.0	194.2	198.4	191.4	192.7	194.2
96.0	193.3	200.6	193.7	193.7	195.3
95.0	192.6	203.0	195.2	195.4	196.5
94.0	192.1	204.4	195.5	196.4	197.0
93.0	192.0	205.3	195.2	196.7	197.2
92.0	192.7	205.5	194.6	197.3	197.5
91.0	194.8	205.3	192.4	198.2	197.7
90.0	196.7	204.9	189.3	198.9	197.5
89.0	197.7	204.0	187.0	199.2	197.1
88.0	198.7	202.4	186.0	199.0	196.6
87.0	202.0	200.5	186.2	198.9	197.1
86.0	205.7	197.4	187.2	199.3	197.6
85.0	209.0	196.3	190.8	202.0	199.6
84.0	212.4	199.7	197.7	206.5	204.0
83.0	216.0	206.9	207.5	213.7	210.9

Table 3. Monthly and Annual Mean Temperature (K) at SOR

Altitude, km	January	February	March	April	May	June	August	September	October	November	December	Annual
105.0	201.8	209.8	198.4	202.9	200.7	227.0	220.3	209.7	206.7	195.5	190.9	207.5
104.0	195.1	200.5	193.9	190.3	195.3	216.8	211.0	200.6	196.9	190.9	186.9	199.6
103.0	187.7	194.3	189.8	184.6	194.8	206.9	199.5	192.6	190.0	187.0	183.9	193.1
102.0	183.8	188.1	186.5	180.2	193.8	199.1	194.4	189.7	186.4	183.1	182.5	189.0
101.0	181.9	183.7	186.6	180.0	193.4	194.6	192.2	189.6	184.8	180.8	181.6	187.1
100.0	181.1	181.5	189.4	181.8	192.9	191.8	191.6	191.8	184.4	180.9	181.9	186.9
99.0	181.6	181.2	191.9	185.2	192.9	189.6	191.4	194.2	185.4	182.1	183.0	187.5
98.0	183.7	182.2	194.0	189.5	192.9	185.6	191.7	196.4	187.6	183.6	185.5	188.5
97.0	185.8	184.5	196.3	193.7	193.2	181.9	191.3	197.8	189.3	185.6	188.9	189.5
96.0	187.8	187.1	198.8	197.1	193.2	180.6	191.3	198.7	191.2	187.8	192.3	190.9
95.0	189.8	189.5	201.8	200.0	192.4	181.1	191.5	200.0	192.6	190.0	195.3	192.3
94.0	191.8	191.5	205.1	202.4	191.4	182.3	191.8	201.2	194.0	192.1	198.0	193.8
93.0	194.3	192.6	207.1	202.5	191.5	183.3	192.8	201.5	196.0	193.7	200.0	195.0
92.0	197.2	193.1	207.0	200.3	191.6	182.8	193.1	200.7	198.6	196.5	201.9	195.6
91.0	199.8	195.1	205.9	197.9	190.7	182.9	192.2	199.3	200.8	200.4	203.6	196.1
90.0	202.3	197.2	205.0	196.4	189.4	183.2	191.0	198.0	203.0	204.5	204.1	196.5
89.0	204.7	196.8	204.7	195.5	188.8	181.8	188.1	197.0	205.4	208.5	203.1	196.2
88.0	205.9	194.3	203.8	194.1	188.8	178.5	182.9	194.9	206.3	211.8	201.7	194.8
87.0	204.9	193.0	201.6	192.7	189.2	176.1	178.6	193.4	205.6	214.4	200.8	193.5
86.0	202.3	193.0	198.3	191.0	189.5	175.9	178.0	193.9	205.2	215.3	199.4	192.8
85.0	199.9	195.4	196.7	191.0	189.5	177.0	181.2	195.1	205.0	213.8	199.3	193.2
84.0	198.9	199.6	196.1	193.2	189.0	181.4	184.8	197.4	203.4	212.5	200.1	194.6
83.0	199.7	205.3	199.3	197.3	190.8	189.2	188.2	200.3	202.4	213.0	202.4	197.7
82.0	203.4	210.2	203.5	202.9	196.0	197.5	193.2	203.8	205.6	214.1	206.4	202.4

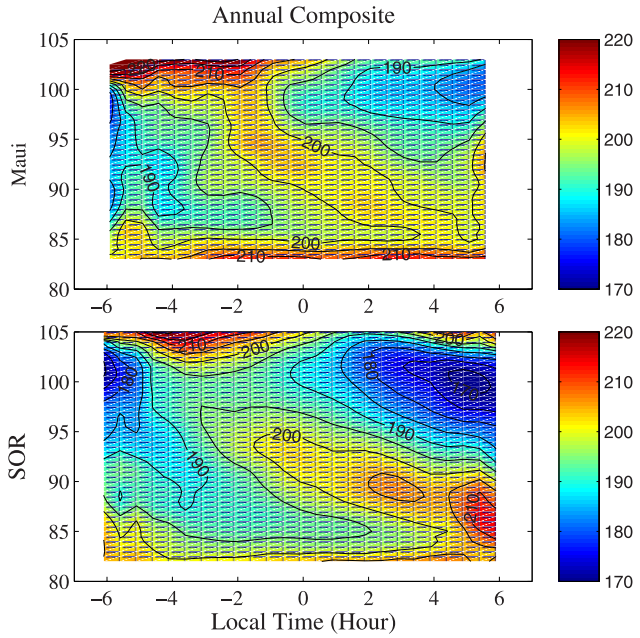

Figure 6. Annual composite night data for Maui and SOR. The annual data were obtained by averaging the monthly composite nights (shown in Figure 3) over 4 months at Maui and 11 months at SOR.

MSIS-00 in January and February, colder than the MSIS-00 in April, May, September, October, November, and December, and are consistent with the MSIS-00 in March, June, and August. One interesting point is that the SOR temperature in May is almost flat between 83 km and 103 km, which is completely different from the MSIS-00 prediction.

[14] Different discrepancies occur at Maui where the lidar temperatures are generally warmer than the MSIS-00 predictions as shown in Figure 5. Particularly in October, the observed temperatures are much warmer than the MSIS-00 model outside the inversion layers. In January, the Maui lidar data show a weak inversion layer from 93 to 100 km, but the observed temperature is about 20 K warmer than the MSIS-00 around 98 km. It is interesting that the MSIS-00 model predicts the January mesopause to be colder than in July at Maui, while the lidar observations show the opposite.

4.2. Comparison Between SOR and Maui

[15] The January, April, July, and October monthly mean temperature profiles at Maui and SOR are compared in Figure 8. Owing to the lack of July data at SOR, the June and August means were averaged and plotted as the dashed line in Figure 8c. Although the MLT profiles at both sites exhibit the temperature inversion layers and two temperature minima, there are significant differences between SOR and Maui. In order to characterize the inversion layers, we draw a straight line from the upper minimum to the lower minimum on the temperature profile for each month, and then compute the temperature differences between the actual temperature profile and this straight line. The maximum temperature difference is defined as the amplitude of the MIL enhancement above the mean background, and the corresponding location is defined as the peak altitude of the MIL. The MIL width is defined as the separation between the lower minimum and the upper minimum. The computed MIL parameters are listed in Table 5 for each month at SOR and Maui. Also listed are the means and standard deviations of these parameters. Two major differences between SOR and Maui can be seen from this table. First, at SOR the amplitudes of the MILs are much larger than the corresponding Maui amplitudes. Particularly in January and October, the SOR MIL amplitudes are approximately 10 K while the Maui MILs are only about 2 K. The mean amplitude at SOR is 9.8 K, which is almost double of the mean amplitude at Maui (~5.8 K). Second, the inversion layers are much wider at SOR than at Maui. This is obvious in January and October when the SOR MIL widths are 16 and 17.5 km, respectively, in contrast with the Maui widths of only 8 and 10.5 km. In addition, the peak of SOR MIL is a few kilometers lower than the Maui MIL. The largest MIL amplitude occurs in April at both SOR and Maui with 17.7 and 10.6 K, respectively. Owing to the nearly flat region between 83 and 103 km, the MIL amplitude in May is extremely small (~1.5 K) at SOR.

[16] The differences between SOR and Maui are also clearly shown in the annual mean temperature profiles (Figure 7). The Maui annual mean is warmer than at SOR throughout the entire MLT region (80–105 km): warmer by 1–4 K between 86 and 98 km and by 4–15 K outside this range. The mesopause for the SOR annual mean profile is at 100.5 km with a temperature of 187 K, while the mesopause for the Maui annual mean is at 98.5 km with a warmer temperature of 193 K. The lower minimum of the SOR annual mean is at 85.5 km with a temperature of 192.5 K while the lower minimum for the Maui annual mean is at 88 km with a temperature of 196.6 K. The Maui MILs have a smaller width (~11 km) than the SOR MILs (~15 km).

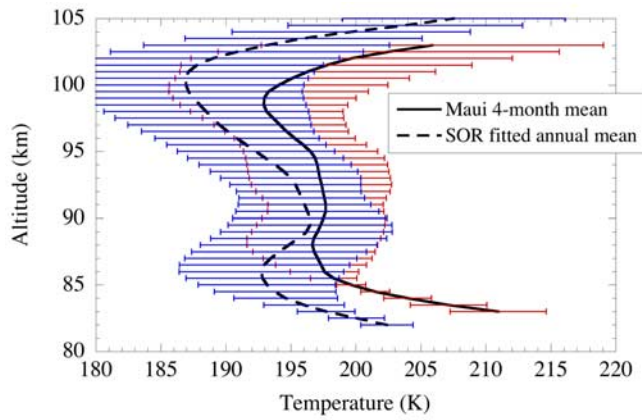

Figure 7. Comparison of Maui and SOR nocturnal annual mean. The Maui annual mean was obtained by averaging the 10 hours of the annual composite night data shown in Figure 6, while the SOR annual mean was derived from a harmonic fit to the 11 monthly means of SOR lidar temperatures. Numerical values of these annual mean temperatures are listed in Tables 3 and 4 for SOR and Maui, respectively. The horizontal lines spanning the annual mean profiles indicate the geophysical variability derived from the standard deviation of the annual composite nights shown in Figure 6. Here the blue lines are for SOR, while the red are for Maui.

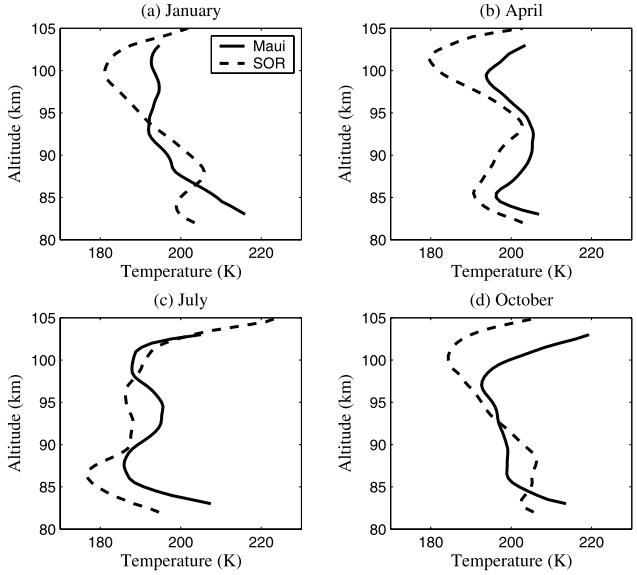

Figure 8. Comparison of Maui and SOR nocturnal monthly means. The SOR July mean was derived by averaging the SOR June and August means.

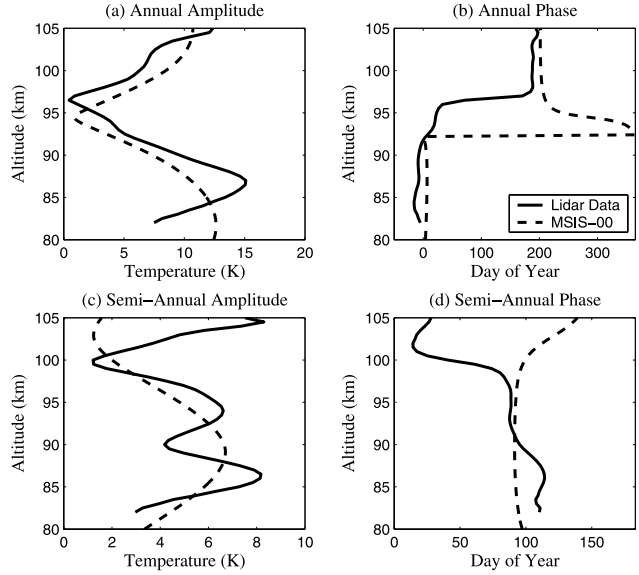

Figure 9. Comparison of annual and semiannual amplitudes and phases between the SOR lidar data (solid curves) and the MSIS-00 model (dashed curves).

The amplitude of the Maui MIL is only about half of the amplitude of the SOR MIL.

[17] Significant differences between SOR and Maui occur in October. The Maui October monthly mean is more than 10 K warmer compared to SOR in the range outside the temperature inversion layers (Figure 8d). Such warm Maui temperatures can also be seen in Figure 3d. Warm temperatures occur below 85 km and above 97 km throughout the whole night at Maui.

5. Seasonal Temperature Variations

5.1. Annual and Semiannual Variations

[18] As described in section 4, the mean plus annual and semiannual sinusoidal variations were computed at each altitude in the MLT region using a harmonic fit to the 11 monthly mean temperature profiles measured at SOR. The amplitudes and phases of these harmonic variations are plotted in Figure 9 as the solid curves. The SOR seasonal variation is dominated by an annual variation whose amplitude is approximately double that of the semiannual amplitude throughout the 80–105 km range. The maximum amplitude (~14 K) for the annual variation occurs at 87 km while its minimum (~1 K) occurs at 96 km. There is a large phase jump around 96 km. Below this altitude, the annual variation peaks (warmer) in midwinter, while above this altitude the annual variation peaks in midsummer. We applied the same harmonic fit to the MSIS-00 nighttime predictions and the results are plotted in Figure 9 as dashed curves. The annual amplitude and phase of the MSIS-00 model are similar to the SOR lidar measurements. Some differences between the MSIS-00 and the SOR lidar data exist in the semiannual amplitude and phase, especially above 100 km. The lidar data show much larger amplitude and almost opposite phase to the MSIS-00 model.

[19] The Maui annual variation is characterized by applying a harmonic fit to the 4 months of lidar data. The fitting equation contains a mean plus an annual sinusoidal variation. Plotted in Figure 10 are the amplitude and phase of the measured annual variations along with the MSIS-00 predictions at Maui. The peak amplitude (~10 K) occurs near 86 km while the minimum (~3 K) occurs between 96 and 98 km. In general, the annual amplitude at Maui is smaller than at SOR. This is expected because the annual variations of the solar and the dynamic forcing are smaller in the subtropics than at midlatitudes [*Andrews et al.*, 1987].

Table 5. Parameters of the Mesospheric Temperature Inversion Layers at SOR and Maui

	January	February	March	April	May	June	July	August	September	October	November	December	Mean ± Standard Deviation
							Altitude, km						
SOR	88.5	90	93	93.5	92	90	—	90.5	93.5	88.5	87	91	90.7 ± 2.2
Maui	98	—	—	92.5	—	—	94.5	—	—	90	—	—	93.8 ± 3.4
							Amplitude, K						
SOR	11.6	7.6	16.3	17.7	1.5	5.7	—	9.7	10.0	9.4	7.7	10.7	9.8 ± 4.5
Maui	2.2	—	—	10.6	—	—	8.5	—	—	2.0	—	—	5.8 ± 4.4
							Width, km						
SOR	16	13	17.5	16	10	9.5	—	13	14.5	17.5	16.5	15.5	14.5 ± 2.8
Maui	8	—	—	14.5	—	—	11.5	—	—	10.5	—	—	11.1 ± 2.7

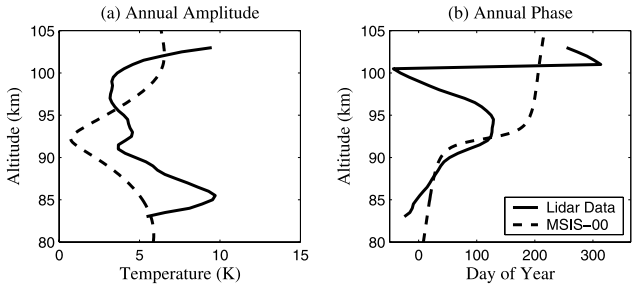

Figure 10. Comparison of annual amplitudes and phases between the Maui lidar data (solid curves) and the MSIS-00 model (dashed curves).

5.2. Variations of the Mesopause

[20] To further characterize the SOR seasonal variations, the mean plus the annual and semiannual harmonic fits were subtracted from the measured SOR lidar temperatures and the residuals were smoothed using a Hamming window with a FWHM of 6 weeks and a time resolution of 1 day. The smoothed residual temperature (with 1-day resolution) was then added back to the mean plus annual and semiannual harmonic fits. The resulting seasonal variations of the MLT temperature for SOR are plotted in Figure 11. An obvious feature is the low mesopause altitude (~86 km) in the summer and the high mesopause altitude (~100 km) in the rest of the year. The mesopause, defined as the altitude of the absolute minimum temperature between the mesosphere and the thermosphere after sufficient averaging to smooth out most of the wave effects [*She and von Zahn*, 1998], was determined for every single day throughout the year from the smoothed SOR data shown in Figure 11 and the results are plotted in Figure 12 as solid lines. Also plotted are the mesopause altitude and temperature determined from the SOR monthly mean profiles (the open circles) for comparison. Since the wave perturbations have significant effects on temperature, it is important to eliminate most wave effects before determining the mesopause locations. Unlike some other analyses that determine the mesopause from individual observational nights [e.g., *Friedman*, 2003], the SOR mesopause shown as the solid line in Figure 12 is derived from the fitted and smoothed seasonal data (shown in Figure 11). The fitting and smoothing removed most of the waves except the diurnal tides. Thus we believe that the SOR mesopause derived here may represent the actual SOR nocturnal mesopause better than using individual nightly profiles.

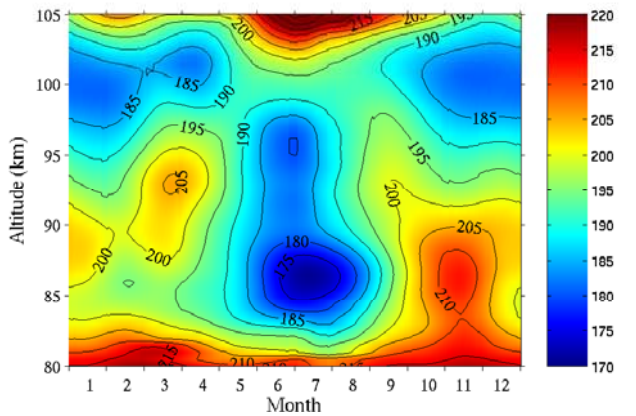

Figure 11. Seasonal variations of SOR nocturnal temperature in the MLT region. See text for details.

5.2.1. Mesopause Altitude

[21] At SOR the mesopause is located near 101 km from January to April, then rapidly descends to about 86.5 km at the beginning of May and remains there until the end of August. In early September the mesopause abruptly switches back to its high level of 101 km and remains there until late April. This mesopause altitude feature qualitatively agrees with the previous lidar measurements in the middle and high latitudes [*von Zahn et al.*, 1996; *She and von Zahn*, 1998; *States and Gardner*, 2000; *She et al.*, 2000; *Pan and Gardner*, 2003], but the transition periods are different from another midlatitude location at Urbana. The Urbana diurnal mean data show an abrupt transition of the mesopause altitude from high (98–101 km) to low (86–88 km) in early May. The mesopause then remains at the low altitude for about 70 days until mid-July when it abruptly moves to ~96 km and then slowly increases over the next several months back to the high state (~101 km) [*States and Gardner*, 2000]. Compared with the diurnal mean, the nighttime mesopause moves to the low altitude earlier in the spring (early April) and remains there longer (almost double that for

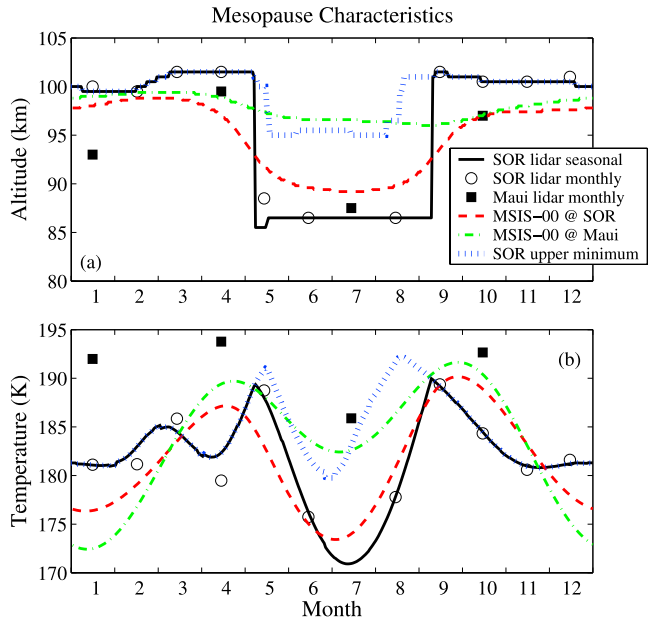

Figure 12. Annual variations of the nocturnal mesopause altitude and temperature at SOR (35.0°N) and Maui (20.7°N). The solid curves are from the SOR seasonal temperature shown in Figure 11, the open circles are from the SOR monthly means of lidar temperatures, the closed squares are from the Maui monthly means of lidar temperatures, the red dashed lines are from the MSIS-00 nightly mean data at SOR, and the green dash-dot lines are from the MSIS-00 nightly mean data at Maui. Also plotted are the altitude and temperature of the upper minimum obtained from the SOR seasonal temperature as the blue dotted curves.

the diurnal mean) until mid-August when it abruptly moves back to the 101 km [*States and Gardner*, 2000]. We also computed the daily mesopause from the 10-hour nightly mean MSIS-00 model for SOR and plotted the results as the red dashed curves in Figure 12. Although the MSIS-00 model also predicts a low altitude mesopause in the summer and a high altitude in the winter, there are two obvious differences between the MSIS-00 predictions and the lidar data. First, the MSIS-00 exhibits two transition periods of April–May and August–September in which the mesopause altitude changes smoothly from one level to another, while the lidar data show two abrupt transitions. Second, the two levels of about 98 and 88 km in MSIS-00 model are different from the two levels of about 101 and 86.5 km revealed in the SOR lidar data. In other words, the separation between the two levels in MSIS-00 model is smaller than the separation in the SOR lidar data by about 4 km.

[22] The Maui mesopause altitude and temperature were determined from the monthly mean temperature profiles (Figure 5) and plotted as the closed squares in Figure 12. A distinguished feature of the Maui lidar measurements is the low mesopause altitude (~87.5 km) in July, which is similar to the SOR results but contradictory to the MSIS-00 predictions and previous lidar measurements in the tropics and subtropics [*von Zahn et al.*, 1996; *Clemesha et al.*, 1999; *Friedman*, 2003]. According to the MSIS-00 model, the variation of the mesopause altitude at Maui is from a winter high of 99 km to a summer low of 96 km with smooth transitions like the SOR predictions. Previous lidar measurements seem to agree with the Maui predictions. *She and von Zahn* [1998] suggested that the mesopause is probably always located around 100 km in the tropics and subtropics (between 23°S and 23°N) based upon the ship-borne K lidar measurements across the equator [*von Zahn et al.*, 1996]. *Clemesha et al.* [1999] reported temperature profiles measured by a Na lidar at Sao Jose dos Campos, Brazil (23°S, 46°W) between July and October 1998 (from winter through spring equinox at this southern location). A high mesopause altitude around 100 km was observed during this period. *Friedman* [2003] made a systematic study of the mesopause at Arecibo, Puerto Rico (18.35°N, 66.75°W) with a K lidar. The mesopause stays in an altitude range of 95–105 km through most of the year, even in the summer. Only 3 of 29 nights from May to August have mesopause altitude below 95 km, but there is a cluster of mesopause height between 90 and 95 km in February.

5.2.2. Tidal Influences on Mesopause and Inversion Layers

[23] Owing to the mesospheric temperature inversion layers, two temperature minima are typically present in the nighttime MLT region. By definition, the mesopause is the minimum with the lowest temperature. As illustrated in Figure 5, at Maui the lower minimum is 1 K colder than the upper minimum in January and 3 K colder in July. Thus the lower minimum should be the mesopause in these two months as a consequence. Such small temperature differences mean that perturbations associated with tides and gravity waves could reverse the situation and move the mesopause by 10 km or more in timescale of tens of minutes to hours. As pointed out earlier in section 4, the composite nights in Figure 3 remove most of the noncoherent waves like gravity waves, but cannot remove coherent tides. Tidal variations are clearly shown in Figure 3 for both SOR and Maui. To examine the tidal influences on the mesopause altitude and the temperature inversion layers, we performed a semidiurnal tidal fit (a mean plus a 12-hour sinusoidal variation) to the Maui monthly composite nights shown in Figure 3. The derived semidiurnal tides (without the mean) are plotted as a function of local time and altitude in the middle panel of each subplot in Figure 13 for each month. We then subtracted the obtained semidiurnal tides from the original monthly composite nights to derive the "background" thermal structure. The resulting monthly "background" composite nights are plotted in the top panel of each subplot in Figure 13.

[24] Except during October, the tidal signature with downward phase propagation nearly disappears from the "background" composite nights in January, April, and July at Maui; while the tidal signature is well reproduced in corresponding semidiurnal tide plots. This indicates that semidiurnal tides are dominant in these three months at Maui, but much weaker in October. With the 12-hour tides removed from the original composite nights, the "background" composite night in Figure 13c clearly shows that the mesopause (i.e., the absolute minimum temperature between the mesosphere and the thermosphere) resides around 87–88 km through most of the night in July at Maui. This is significantly different from the original data shown in Figure 3c where the lowest temperature minimum is near 87.5 km at the beginning of the night, and then switches to a higher altitude around 100 km after local midnight. Similar situation occurs in April at Maui. The original composite night shown in Figure 3b suggests that the mesopause is in between 85 and 90 km at the beginning of the night and then increases to around 100 km in the late night. In contrast, the new "background" composite night in Figure 13b indicates that the mesopause stays around 100 km through most of the night in April at Maui. In addition, the "background" composite nights in Figure 13 also clearly show the temperature inversion layers through the whole nights in April and July at Maui.

[25] We then took the monthly mean temperature from the "background" composite nights using the same method for the original monthly mean as described in section 4, i.e., averaging over the 10-hour period centered about local midnight. The new "background" monthly mean is plotted as the solid curve in the bottom panel of each subplot in Figure 13, while the original monthly mean (the same as Figure 5) is plotted as the dashed curve in the same panel for comparison. The new "background" monthly means are almost identical to the original means in April and October, but differ in January and July with a little colder mesopause temperatures and a little warmer upper minimum than the originals. Thus the "background" monthly means exhibit more pronounced mesopause location at 92 km in January and at 87.5 km in July. The temperature inversion layers in the new "background" monthly means are as strong as those in the original monthly means. This result is expected since our original 10-hour average through the original composite nights has removed most of the 12-hour tides, thus, the new monthly means would not be much different from the originals. The above results also suggest that the semidiurnal tides are ruled out to be the cause for the temperature inversion layers and for the difference in the

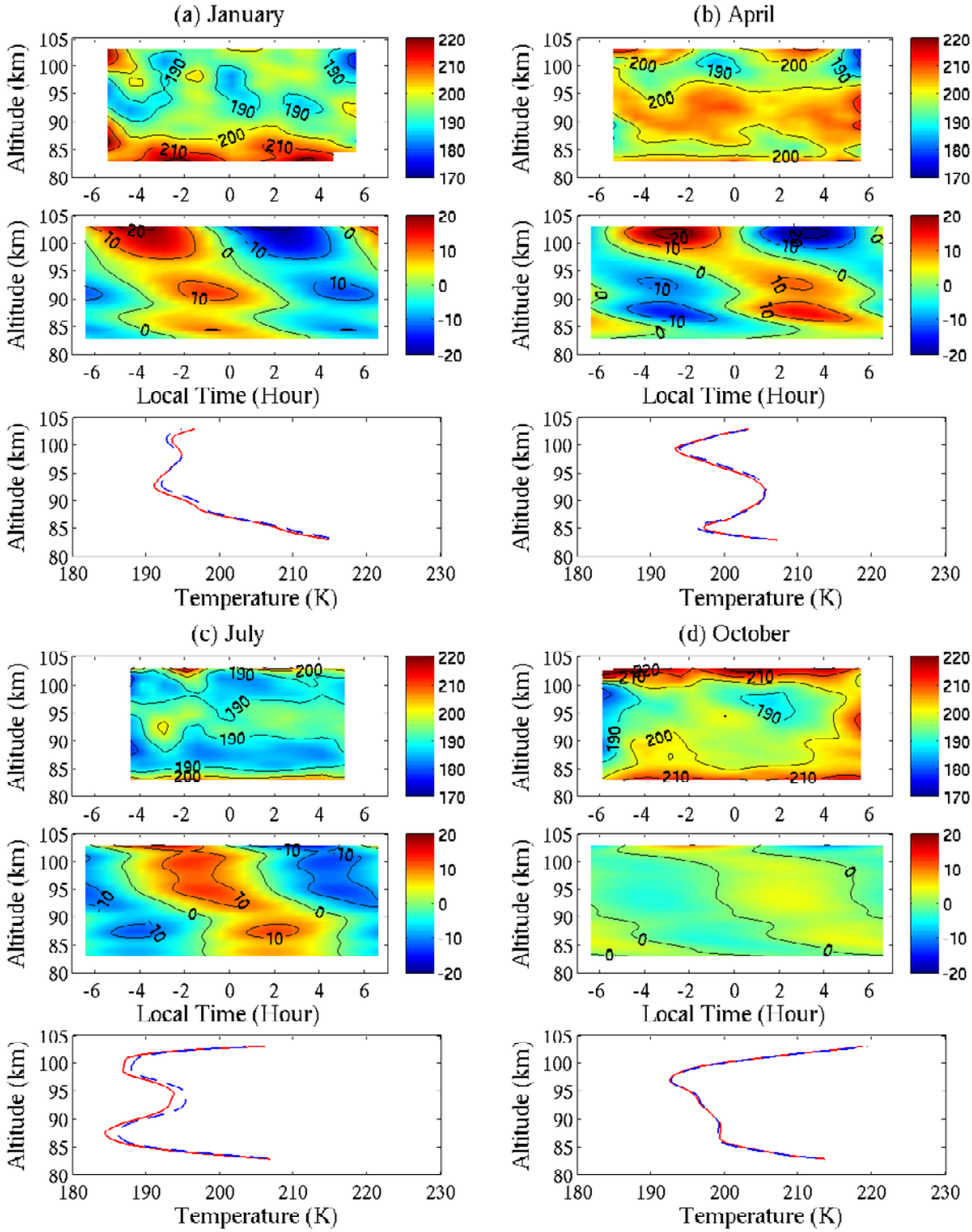

Figure 13. Examination of the semidiurnal tidal influence on the background thermal structure in the four months at Maui. For the subplot of each month the top panel exhibits the background composite night temperatures after subtracting the semidiurnal tide from the data shown in Figure 3; the middle panel shows the derived semidiurnal tide; and the bottom panel plots the monthly mean temperature profiles before (dashed curve) and after (solid curve) the subtraction of the semidiurnal tides.

July mesopause altitude found between our lidar measurements at Maui and other groups at other tropical and subtropical locations. Likely, the 24-hour diurnal tide is mainly responsible for the mesopause altitude difference and the temperature inversion layers [*States and Gardner*, 2000]. In addition, other perturbations like the nonmigrating tides may be partially responsible for the low mesopause altitude in July at Maui, since these nonmigrating tides are known to be strong in the tropics and subtropics [*Talaat and Lieberman*, 1999].

[26] Caution must be taken when interpreting the semidiurnal tides obtained from the 12-hour tidal fitting to the 10-hour nighttime data, since it is possible that part of the 12-hour tidal amplitude is from the leakage of the 24-hour tidal variations being truncated to 10 hours. It is beyond the scope of this paper to estimate the possible amplitude of this leakage since we do not have the information of the diurnal tide amplitude. Therefore the semidiurnal tides derived from the fitting as well as the resulted "background" composite nights (shown in Figure 13) should only be used for comparison purposes. We do not claim that these composite nights and their corresponding monthly mean temperatures (in Figure 13) represent the true nocturnal thermal structure. However, Figure 13 indicates that the original monthly mean temperatures (in Figures 4 and 5) derived from the average of the 10-hour original composite nights are good representations of the nocturnal thermal structure at both sites.

5.2.3. Mesopause Temperature

[27] As shown in Figure 12b, the SOR mesopause temperature is coldest in the midsummer (~171 K), and warmest in early May and early September (~190 K). The amplitude of the mesopause temperature variation is about 19 K at this midlatitude site. We noticed a small asymmetry in Figure 12b. The mesopause temperature in early September is a little warmer than in early May. This small asymmetry is also predicted in the MSIS-00 model (red dashed curve). According to the MSIS-00 model, the lowest mesopause temperature occurs in midsummer but there is a 10-day shift relative to the lidar data toward the end of June. The major differences in the lidar and model mesopause temperatures occur in the winter months (December, January, and February). The MSIS-00 predictions are about 5 K colder than the lidar observations in these months. Especially in January, the MSIS-00 predicts a cold mesopause temperature close to the midsummer temperature. This is not the case in the SOR lidar data.

[28] Figure 12b indicates that the Maui mesopause temperatures (closed squares) are generally warmer than the corresponding SOR mesopause by about 10 K. The temperature is coldest in July (~185 K) and warmest in April and October (~194 K). The amplitude of the mesopause temperature variation is about 9 K at Maui, which is about half of the amplitude at SOR. The measured mesopause temperatures are also warmer than the MSIS-00 predictions at Maui (green dash-dot curve in Figure 12b). Especially in January, the difference reaches 20 K. Surprisingly, the MSIS-00 model predicts the mesopause temperature in the winter months (December, January, and February) to be much colder than in July. This is opposite to our lidar observations.

[29] The altitude and temperature of the upper minimum determined from the SOR seasonal temperatures are plotted in Figure 12 as the blue dotted curves. It is interesting to see that the upper minimum is bimodal with a height near 95 km in summer and near 101 km in the rest of the year. The transitions of the upper minimum altitude occur in mid-May and mid-August, which are also abrupt, just like the transitions of mesopause altitude. The variations of temperatures at 86.5 and 101 km through the year are plotted in Figure 14. These are the altitudes corresponding to two temperature minima during the transition period. The temperature lines cross twice during a year and they mark the transitions of the mesopause altitude. These abrupt transitions may be understood as a competition between the upper minimum determined by the radiative balance and the lower minimum around 86.5 km formed by the dynamic forcing [*Andrews et al.*, 1987]. Further discussion about the mesopause temperature and altitude needs theoretical and modeling support, which is beyond the scope of this paper.

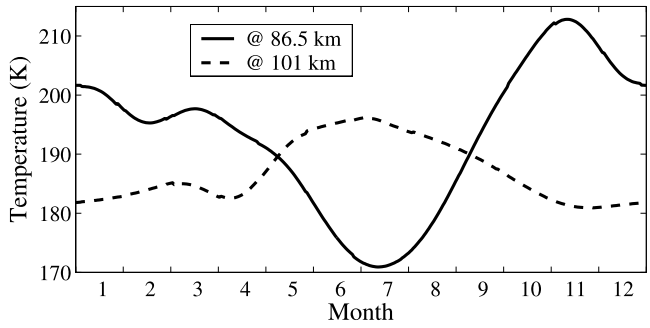

Figure 14. Seasonal variations of the nocturnal temperatures at 86.5 and 101 km at SOR.

6. Conclusions

[30] The nocturnal thermal structure of the MLT region at SOR (35°N) and Maui (20.7°N) are characterized using the Na wind/temperature lidar observations. Mesospheric temperature inversion layers (MIL) and two temperature minima are common features of the nighttime MLT region (80–105 km) at both SOR and Maui. The amplitudes of the Maui MIL enhancement above the MLT mean background (~5.8 K) are only about half of those at SOR (~9.8 K). The Maui inversion layers also have a smaller width of ~11 km, compared to ~15 km at SOR. The SOR nocturnal mesopause temperature is coldest in midsummer around July (~171 K), and warmest in early May and early September (~190 K). The Maui nocturnal mesopause temperature is also coldest in July (~185 K) and warmest in April and October (~194 K). The amplitude (~9 K) of the mesopause temperature variation at Maui is only about half of the amplitude (~19 K) at SOR. This is probably related to the weaker up/down welling motions associated with the meridional circulation and the smaller variation of solar flux from summer to winter in the tropics and subtropics compared to midlatitudes. The Maui mesopause temperatures are warmer than the corresponding SOR mesopause temperatures. The Maui nocturnal monthly means and annual mean are also generally warmer than the corresponding SOR means, especially below 85 km and above 95 km.

[31] Large differences are observed between the lidar data and the MSIS-00 predictions. The MSIS-00 model does not contain any inversion layers and only predicts a single temperature minimum in the nighttime MLT region. The chemical heating effects should be considered in the future MSIS model to match the lidar nighttime observations. Outside the range of the temperature inversion layers, the MSIS-00 predictions are generally comparable with the SOR lidar data but much colder than the Maui lidar data. The amplitude of the mesopause temperature variation predicted by the MSIS-00 model is much larger than the lidar observed amplitude at Maui. The smooth transition of mesopause altitudes from one state to another predicted by the MSIS-00 model contrasts with the observed abrupt transitions at SOR. At SOR the nocturnal mesopause is near 86.5 km from May through August, and near 101 km during the rest of the year. There are abrupt transitions of the mesopause altitude in early May and early September.

[32] At Maui the nocturnal mesopause altitude is near 87.5 km in July, which is much lower than what previous lidar and satellite measurements have revealed in the tropics and subtropics. However, tides strongly influence the MLT temperature and the mesopause structure. The original composite night in July suggests that the lowest temperature is near 87.5 km at the beginning of the night and then switches to a higher altitude around 100 km after local midnight. With the semidiurnal tides removed from the data, the ''background'' composite night indicates that the mesopause (i.e., the lowest minimum temperature) stays at the low altitude through most of the night in July at Maui. Unfortunately, nighttime only data do not allow us to remove the diurnal tides, which complicates the determination of the background MLT thermal structure. Measurements covering a complete 24-hour diurnal cycle are essential for removing the diurnal tides to reveal the true mean background and for studying thermal tides. This has been achieved at midlatitude locations [*States and Gardner*, 2000], but not yet in the tropics and subtropics. This paper calls for the full diurnal observations of thermal structures in the tropics and subtropics.

[33] **Acknowledgments.** The authors would like to appreciate Gary Swenson and Alan Z. Liu for their valuable comments, and acknowledge George Papen, Peter Dragic, and a few students for their help in collecting data. The authors are grateful to the staff at the Starfire Optical Range and the staff at the Maui Space Surveillance Complex for their support during the observational campaigns. This work was supported by NSF grants ATM-97-09921, ATM-00-03198, and ATM-03-38425.

References

Andrews, D. G., J. R. Holton, and C. B. Leovy (1987), *Middle Atmosphere Dynamics*, Elsevier, New York.

Bills, R. E., C. S. Gardner, and C. Y. She (1991), Narrowband lidar technique for sodium temperature and Doppler wind observations of the upper atmosphere, *Opt. Eng.*, *30*, 13–21.

Chen, S., Z. Hu, M. A. White, H. Chen, D. A. Krueger, and C. Y. She (2000), Lidar observations of seasonal variation of diurnal mean temperature in the mesopause region over Fort Collins, Colorado (41°N, 105°W), *J. Geophys. Res.*, *105*(D10), 12,371–12,379.

Clemesha, B. R., I. Veselovskii, P. P. Batista, M. P. P. M. Jorge, and D. M. Simonich (1999), First mesopause temperature profiles from a fixed southern hemisphere site, *Geophys. Res. Lett.*, *26*(12), 1681–1684.

Forbes, J. M. (1995), Tidal and planetary waves, in *The Upper Mesosphere and Lower Thermosphere: A Review of Experiment and Theory*, *Geophys. Monogr. Ser.*, vol. 87, edited by R. M. Johnson and T. L. Killeen, pp. 67–87, AGU, Washington, D. C.

Fricke-Begemann, C., J. Höffner, and U. von Zahn (2002), The potassium density and temperature structure in the mesopause region (80–105 km) at a low latitude (28°N), *Geophys. Res. Lett.*, *29*(22), 2067, doi:10.1029/2002GL015578.

Friedman, J. S. (2003), Tropical mesopause climatology over the Arecibo Observatory, *Geophys. Res. Lett.*, *30*(12), 1642, doi:10.1029/2003GL016966.

Gardner, C. S., X. Tao, and G. C. Papen (1995), Observations of strong wind shears and temperature enhancements during several sporadic Na layer events above Haleakala, *Geophys. Res. Lett.*, *22*, 2809–2812.

Hedin, A. E. (1991), Extension of the MSIS thermosphere model into the middle and lower atmosphere, *J. Geophys. Res.*, *96*(A2), 1159–1172.

Leblanc, T., I. S. McDermid, P. Keckhut, A. Hauchecorne, C. Y. She, and D. A. Krueger (1998), Temperature climatology of the middle atmosphere from long-term lidar measurements at middle and low latitudes, *J. Geophys. Res.*, *103*(D14), 17,191–17,204.

Lübken, F.-J., and U. von Zahn (1991), Thermal structure of the mesopause region at polar latitudes, *J. Geophys. Res.*, *96*(D11), 20,841–20,857.

Kawahara, T. D., C. S. Gardner, and A. Nomura (2004), Observed temperature structure of the atmosphere above Syowa Station, Antarctica (69°S, 39°E), *J. Geophys. Res.*, *109*, D12103, doi:10.1029/2003JD003918.

Meriwether, J. W., X. Gao, V. Wickwar, T. Wilkerson, K. Beissner, S. Collins, and M. Hagan (1998), Observed coupling of the mesospheric inversion layer to the thermal tidal structure, *Geophys. Res. Lett.*, *25*, 1479–1482.

Mlynczak, M. G., and S. Solomon (1993), A detailed evaluation of the heating efficiency in the middle atmosphere, *J. Geophys. Res.*, *98*, 10,517–10,541.

Pan, W., and C. S. Gardner (2003), Seasonal variations of the atmospheric temperature structure at South Pole, *J. Geophys. Res.*, *108*(D18), 4564, doi:10.1029/2002JD003217.

Papen, G. C., W. M. Pfenninger, and D. M. Simonich (1995), Sensitivity analysis of Na narrowband wind-temperature lidar systems, *Appl. Opt.*, *34*, 480–498.

Picone, J. M., A. E. Hedin, D. P. Drob, and A. C. Aikin (2002), NRLMSISE-00 empirical model of the atmosphere: Statistical comparisons and scientific issues, *J. Geophys. Res.*, *107*(A12), 1468, doi:10.1029/2002JA009430.

She, C. Y., and U. von Zahn (1998), Concept of a two-level mesopause: Support through new lidar observations, *J. Geophys. Res.*, *103*(D5), 5855–5863.

She, C. Y., and J. R. Yu (1994), Simultaneous three-frequency Na lidar measurements of radial wind and temperature in the mesopause region, *Geophys. Res. Lett.*, *21*, 1771–1774.

She, C. Y., J. R. Yu, H. Latifi, and R. E. Bills (1992), High-spectral-resolution lidar for mesospheric sodium temperature measurements, *Appl. Opt.*, *31*, 2095–2106.

She, C. Y., J. R. Yu, and H. Chen (1993), Observed thermal structure of a midlatitude mesopause, *Geophys. Res. Lett.*, *20*, 567–570.

She, C. Y., S. Chen, Z. Hu, J. Sherman, J. D. Vance, V. Vasoli, M. A. White, J. Yu, and D. A. Krueger (2000), Eight-year climatology of nocturnal temperature and sodium density in the mesopause region (80 to 105 km) over Fort Collins, CO (41°N, 105°W), *Geophys. Res. Lett.*, *27*, 3289–3292.

States, R. J., and C. S. Gardner (1998), Influence of the diurnal tide and thermospheric heat sources on the formation of mesospheric temperature inversion layers, *Geophys. Res. Lett.*, *25*, 1483–1486.

States, R. J., and C. S. Gardner (2000), Thermal structure of the mesopause region (80–105 km) at 40°N latitude, part I: Seasonal variations, *J. Atmos. Sci.*, *57*, 66–77.

Talaat, E. R., and R. S. Lieberman (1999), Nonmigrating diurnal tides in mesospheric and lower-thermospheric winds and temperatures, *J. Atmos. Sci.*, *56*, 4073–4087.

Von Zahn, U., J. Höffner, V. Eska, and M. Alpers (1996), The mesopause altitude: Only two distinctive levels worldwide?, *Geophys. Res. Lett.*, *23*, 3231–3234.

X. Chu, S. J. Franke, and C. S. Gardner, Department of Electrical and Computer Engineering, University of Illinois at Urbana-Champaign, 1308 West Main Street, 310 CSL, Urbana, IL 61801, USA. (xchu@uiuc.edu)